Electronic Supplementary Material (ESI) for ChemComm.
This journal is © The Royal Society of Chemistry 2018

Supplementary Materials for

Correlating thermochromic and mechanochromic phosphorescence with polymorphs of a complex gold(I) double salt with infinite aurophilicity

Qi Liu,[ab] Mo Xie,[b] Xiaoyong Chang,[b] Qin Gao,[b] Yong Chen*[a] and Wei Lu*[b]

[a] *Key Laboratory of Photochemical Conversion and Optoelectronic Materials, Technical Institute of Physics and Chemistry & University of Chinese Academy of Sciences, Chinese Academy of Sciences, Beijing 100190, P. R. China. E-mail: chenyong@mail.ipc.ac.cn*

[b] *Department of Chemistry, South University of Science and Technology of China, Shenzhen, Guangdong 518055, P. R. China. E-mail: luw@sustc.edu.cn*

Material and Instrumentation

Potassium dicyanoaurate(I) was purchased from Newburyport, MA.. Solvents used for synthesis were of analytical grade unless stated otherwise. Solvents used for nanostructure preparations and photophysical measurements were of HPLC grade. The cationic precursor $[Au(NHC)_2]$ Cl was synthesized according to literature. ^1H NMR spectra were recorded using a Bruker Avance 400 FT-NMR spectrometer. HR-MS (high resolution mass spectra) were obtained on a Thermo Scientific Q Exactive mass spectrometer, operated in heated electrospray ionization (HESI) mode, and coupled with Thermo Scientific Ultimate 3000 system. Samples were dissolved in HPLC grade methanol and a little other solvent like DMF or CH_2Cl_2. Steady-state emission spectra and excitation spectra for solid were recorded on Edinburgh spectrometer FLS-980 equipped with a Xe light source, an MCP-PMT detector in a cooled housing (20 ^oC), which covers a range of 200–870 nm. Solid-state emissions at controlled variable temperature (77–373 K) were recorded with Oxford Instruments liquid nitrogen cryostat accessory. Emission lifetimes were recorded on Hamamatsu compact fluorescence lifetime spectrometer C11367 and the solid samples were excited at 365 nm. Absolute luminescent quantum yields were recorded with Hamamatsu absolute PL quantum yield spectrometer C11347 equipped with an integrating sphere. Fluorescence microscopy images were recorded on Nikon ECLIPSE Ni-U upright microscope using FLS-980 Xe light source through HG fibers. Emission and excitation spectra of single crystals were also measured on microscope using HG fibers. The powder XRD patterns were recorded on a Rigaku Smartlab X-ray diffractometer equipped with 9 kW X-ray generator. The scanning rate was 5 °/min in the 2θ range from 5 ° to 60 °. The diffraction data were collected at 100 K to 298 K on a Bruker D8 Venture single crystal X-ray diffractometer. The SEM micrographs were taken on a ZEISS Merlin scanning electron microscope operating at 2–5 kV. SEM samples were prepared by drop-casting suspensions onto silicon wafers. The excess solvent was removed by a piece of filter paper. TG and DSC measurement were performed with Netzsch STA 449 F3 and TA DSC25, separately. The rate of

temperature ramp was 10 ^{o}C per minute.

Synthesis of the Double Salt

[Au(NHC)$_2$]Cl (0.02 g, 0.038 mmol) dissolved in water (0.5 mL) and potassium dicyanoaurate (0.011 g, 0.038 mmol) dissolved in water (0.5 mL) were mixed and an emissive solid precipitated in a few seconds. The precipitate was filtered after stirring for 10 min and washed thoroughly with water, acetonitrile, and diethyl ether and dried in air to give double salt as a yellow-green solid (22 mg, yield: 78%). Single crystals of double salt for X-ray crystallography were obtained by slow diffusion of ether into a DMF solution and two polymorphs were obtained. ^{1}H NMR (400 MHz, d$_7$-DMF) δ (ppm): 8.76 (s, 4H), 4.21 (s, 12H). HR-MS (ESI): Calcd for $C_{14}H_{16}AuN_8$ $[M]^+$: 493.1163; Found: 493.1165; Calcd for $Au(CN)_2$ $[M]^-$: 248.9732; Found: 248.9729. Elemental Analysis: C 25.89, H 2.17, N 18.87, Found: C 25.44, H 2.07, N 18.99.

Since polymorphs of double salt were observed through single crystals growing, we proposed that powder crystals of an elusive structure in nano- or micro scales could form under some given conditions (Table S1). By changing solvent from water to methanol or acetonitrile, polymorph **A** and polymorph **B** co-precipitated from the solution. When the solvent was water, plate-like polymorph **B** with diameter in micrometers precipitated immediately after cation and anion meeting each other. When methanol or acetonitrile was used as solvent, a mixture of rod-like cyan-emitting and plate-like yellow-green-emitting double salt precipitated (Fig. S1). The growing process was also recorded using fluorescence microscope as video format (see video in Supporting Information). Since the micro-crystal powder of polymorph **A** was always precipitated together with polymorph **B**, the long fiber-like micro-crystals polymorph **A** was separated manually from polymorph **B** using tweezers.

Table S1. Formation of double salt of different luminescence and morphology under different solvents and concentrations.

Concentration	16 mM		5 mM	
Solvent	Water	CH_3OH or CH_3CN	Water	CH_3OH or CH_3CN
Luminescence	Green	Cyan and Green	Green	Cyan and Green
Morphology	Plate	Fiber and Plate	Plate	Fiber and Plate

Table S3. Photophysical data of polymorph **A** and **B** and ground powder **C** at 293 K and 77 K.

	293 K			77 K	
	λ_{em} / nm	τ (ns)	QY (%)	λ_{em} / nm	τ (ns)
Polymorph **A**	490	79	23	475	<1
				520	409
Polymorph **B**	548	309	51	535	<1
				580	494
Ground Powder **C**	580	486	31	535	<1
				595	567
				700	1126

Table S2. X-ray crystallographic data of the single crystals of polymorph **A** at 150 K, polymorph **B** at 100 K, at 150 K, at 200 K, at 225 K, at 250 K and at 298 K.

	Polymorph **A** at 150 K	Polymorph **B** at 100 K	Polymorph **B** at 150 K	Polymorph **B** at 200 K	Polymorph **B** at 225 K	Polymorph **B** at 250 K	Polymorph **B** at 298 K
Empirical Formula	$C_{16}H_{16}Au_2N_{10}$	$C_{16}H_{16}Au_2N_{10}$	$C_{16}H_{16}Au_2N_{10}$	$C_{16}H_{16}Au_2N_{10}$	$C_{16}H_{16}Au_2N_{10}$	$C_{16}H_{16}Au_2N_{10}$	$C_{16}H_{16}Au_2N_{10}$
Formula Weight	742.32	742.32	742.32	742.32	742.32	742.32	742.32
Crystal System	Monoclinic	Orthorhombic	Orthorhombic	Orthorhombic	Orthorhombic	Orthorhombic	Orthorhombic
Crystal Size	0.34×0.28×0.03	0.3×0.06×0.01	0.3×0.06×0.01	0.3×0.06×0.01	0.3×0.06×0.01	0.3×0.06×0.01	0.3×0.06×0.01
Space Group	C2/m	$Pmn2_1$	$Pmn2_1$	$Pmn2_1$	Pmna	Pmna	Pmna
a (Å)	13.0911(14)	6.2753(7)	6.2961(6)	6.3306(4)	6.3484(4)	6.3632(4)	6.3929(4)
b (Å)	6.4907(7)	8.0957(10)	8.1146(8)	8.1410(5)	8.1538(6)	8.1603	8.1734(6)
c (Å)	11.9991(14)	18.757(2)	18.7357(17)	18.7077(11)	18.6895(12)	18.6843(12)	18.6898(12)
α (°)	90.00	90.00	90.00	90.00	90.00	90.00	90.00
β (°)	105.112(4)	90.00	90.00	90.00	90.00	90.00	90.00
γ (°)	90.00	90.00	90.00	90.00	90.00	90.00	90.00
V ($Å^3$)	984.31(19)	952.93(19)	957.21(16)	964.15(10)	967.44(11)	970.19(11)	976.57(11)

Z Value	2	2	2	2	2	2	2
D_{calc} / g cm^{-3}	2.505	2.587	2.576	2.557	2.548	2.541	2.524
Temperature / K	150	100	150	200	225	250	298
No. of Reflections	11074	23319	17919	18339	18600	18401	18575
Measured	Unique: 894 R_{int} = 0.0710	Unique: 4134 R_{int} = 0.0587	Unique: 2582 R_{int} = 0.0519	Unique: 2603 R_{int} = 0.0543	Unique: 1306 R_{int} = 0.0590	Unique: 1312 R_{int} = 0.0590	Unique: 1321 R_{int} = 0.0653
Goodness of Fit	1.052	1.120	1.256	1.222	1.268	1.276	1.078
Residuals: R_1 (I > 2.00σ (I)) / %	2.63	3.85	4.16	4.40	7.94	7.18	6.99
Residuals: wR_2 (All reflections) / %	7.86	9.20	10.81	11.58	17.21	18.81	19.33
Maximum peak in Final Diff. Map / Å^3	1.246 e$^-$	2.482 e$^-$	3.526 e$^-$	2.279 e$^-$	3.908 e$^-$	2.064 e$^-$	2.263 e$^-$
Minimum peak in Final Diff. Map / Å^3	−1.290 e$^-$	−1.660 e$^-$	−1.825 e$^-$	−2.267 e$^-$	−2.488 e$^-$	−1.585 e$^-$	−1.331 e$^-$

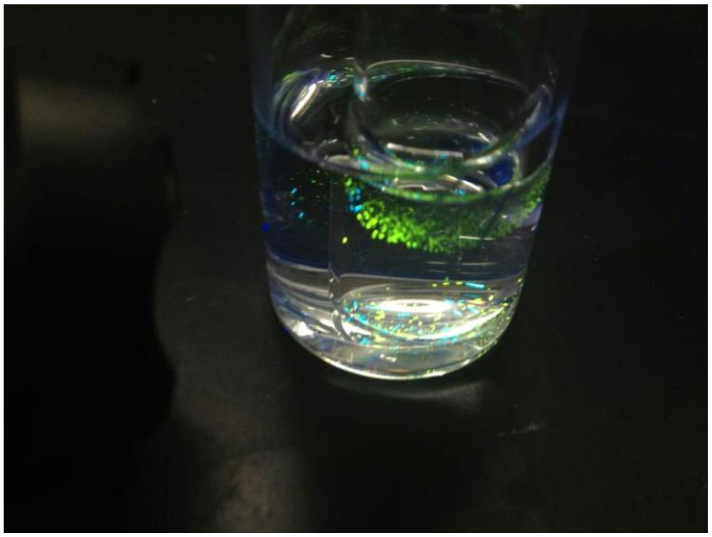

Figure S1. Single crystals of cyan emitting polymorph **A** and green emitting polymorph **B** (under 365 nm UV light) by diffusion of ether into DMF solution at 298 K.

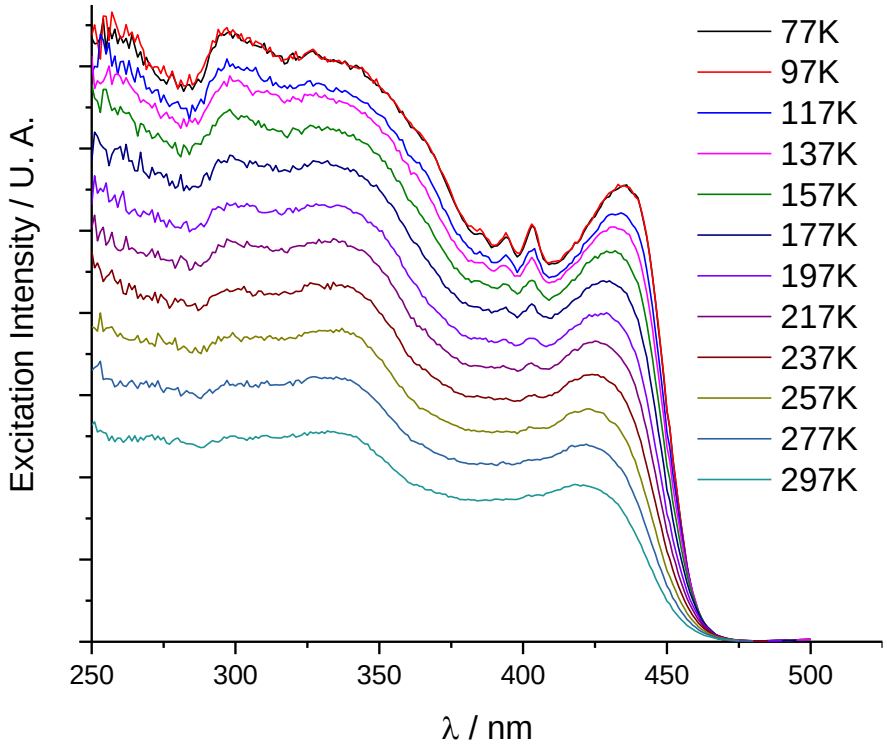

Figure S2. Variable-temperature excitation spectra of polymorph **A** upon monitored at 488 nm.

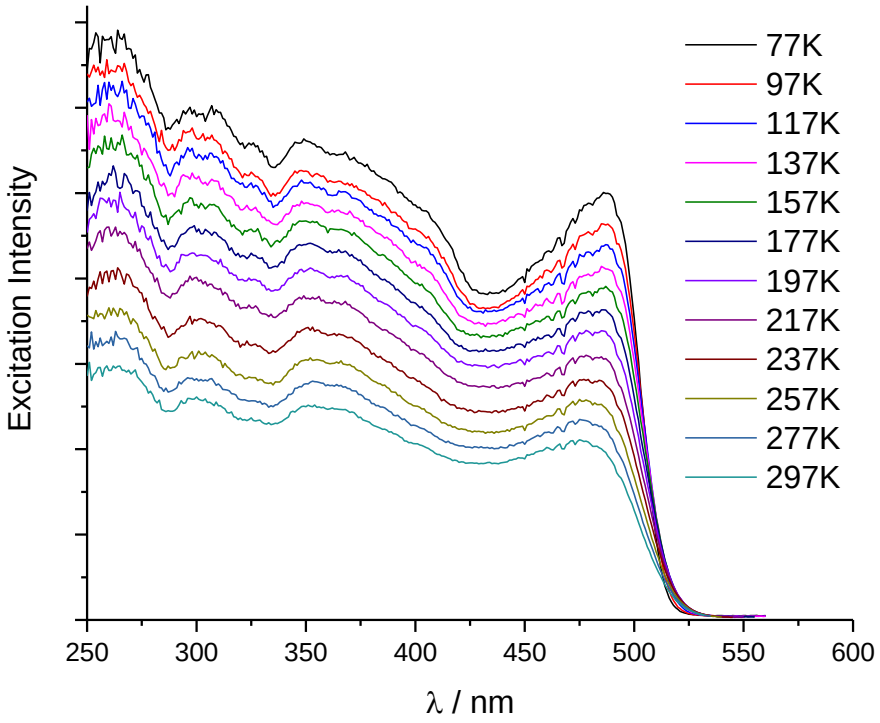

Figure S3. Variable-temperature excitation spectra of polymorph **B** upon monitored at 541 nm.

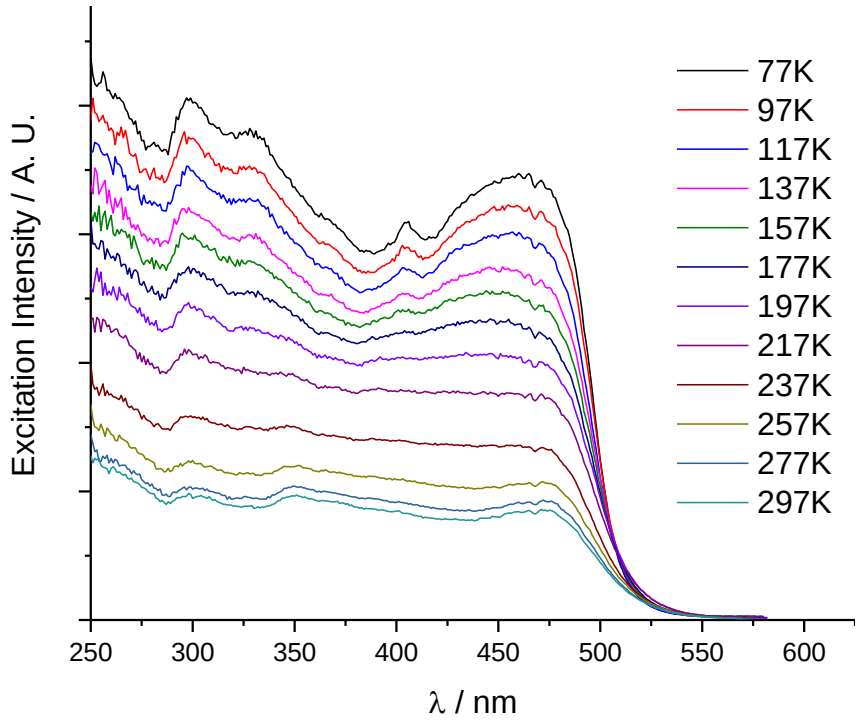

Figure S4. Variable-temperature excitation spectra of ground powder **C** upon monitored at 580 nm.

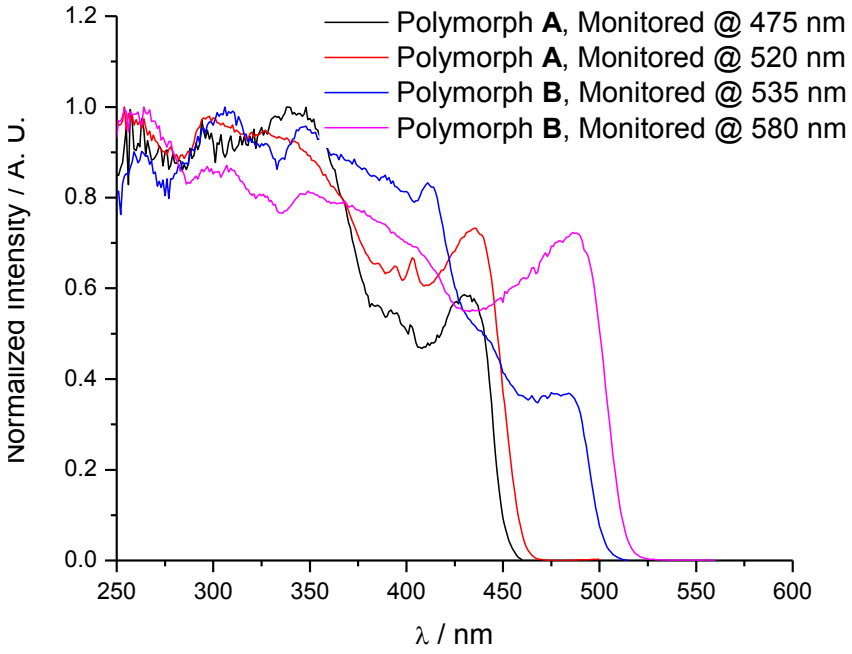

Figure S5. Excitation spectra of polymorph **A** and polymorph **B** at 77 K monitored at a variety of emission wavelength.

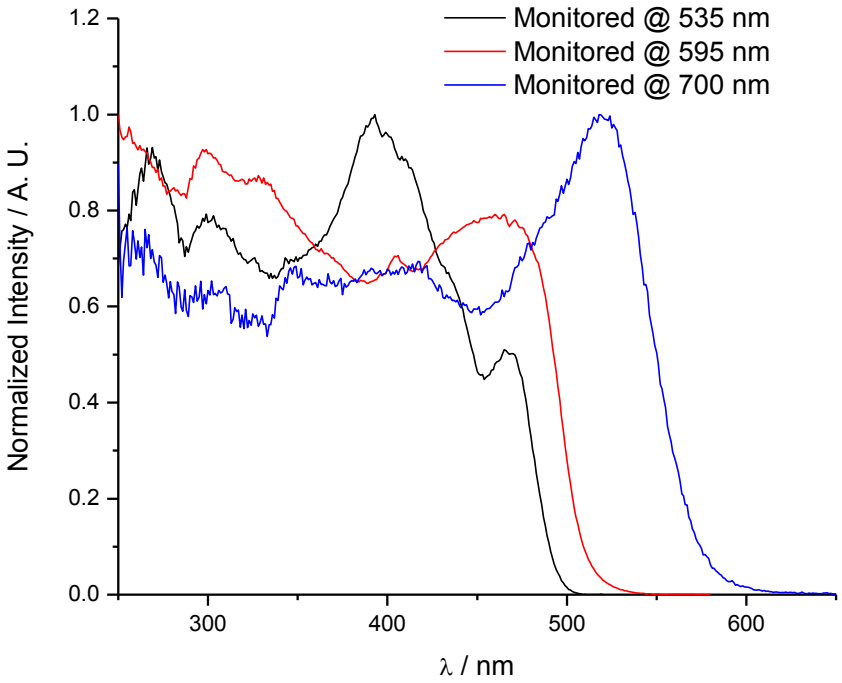

Figure S6. Excitation spectra of ground powder **C** at 77 K monitored at a variety of emission wavelength.

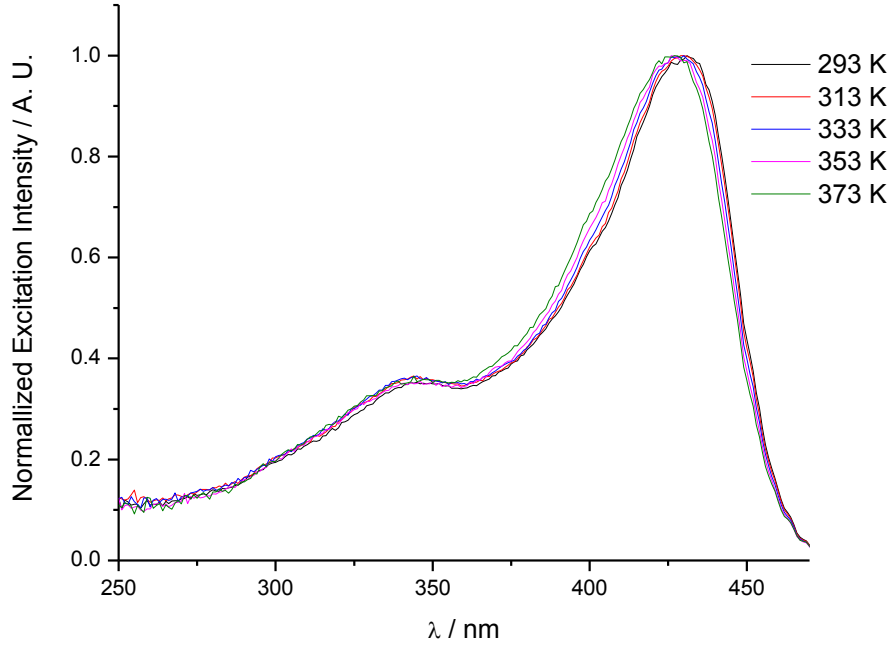

Figure S7. Variable-temperature (293 K to 373 K) excitation spectra of polymorph **A** upon monitored at 490 nm.

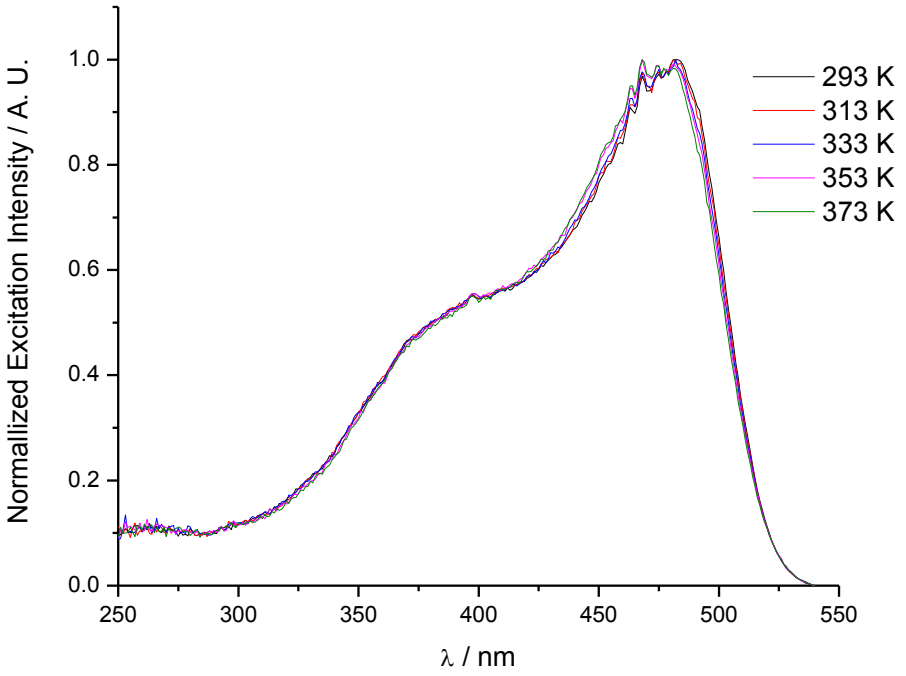

Figure S8. Variable-temperature (293 K to 373 K) excitation spectra of polymorph **B** upon monitored at 548 nm.

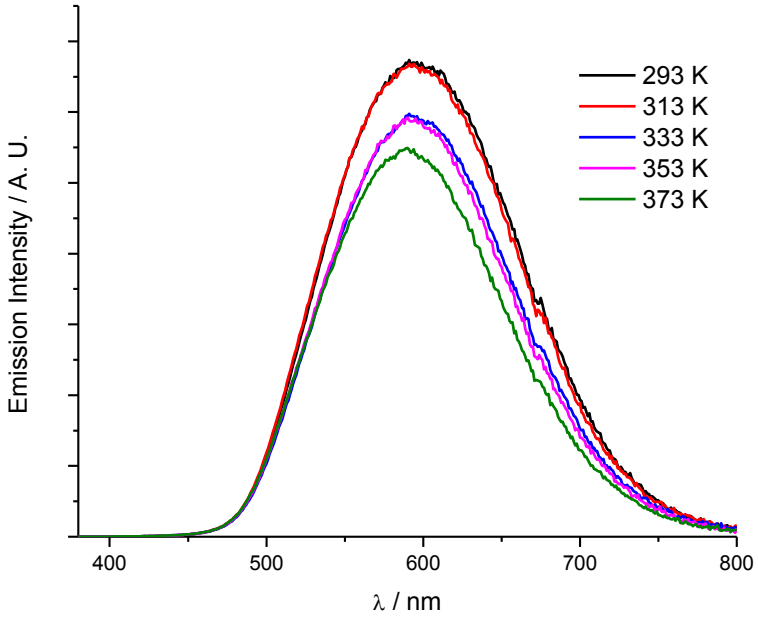

Figure S9. Variable-temperature (293 K to 373 K) emission spectra of ground powder **C**.

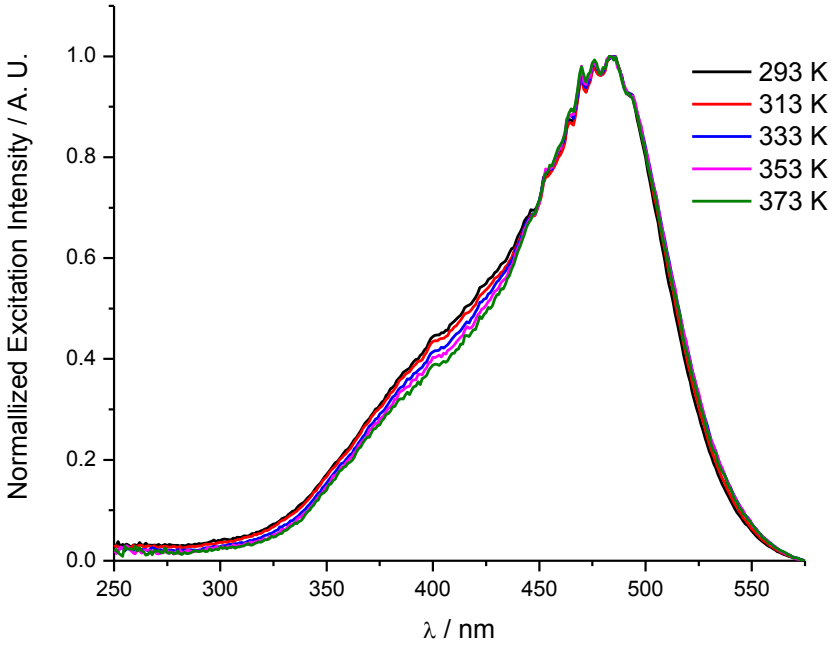

Figure S10. Variable-temperature (293 K to 373 K) excitation spectra of ground powder **C** upon monitored at 580 nm.

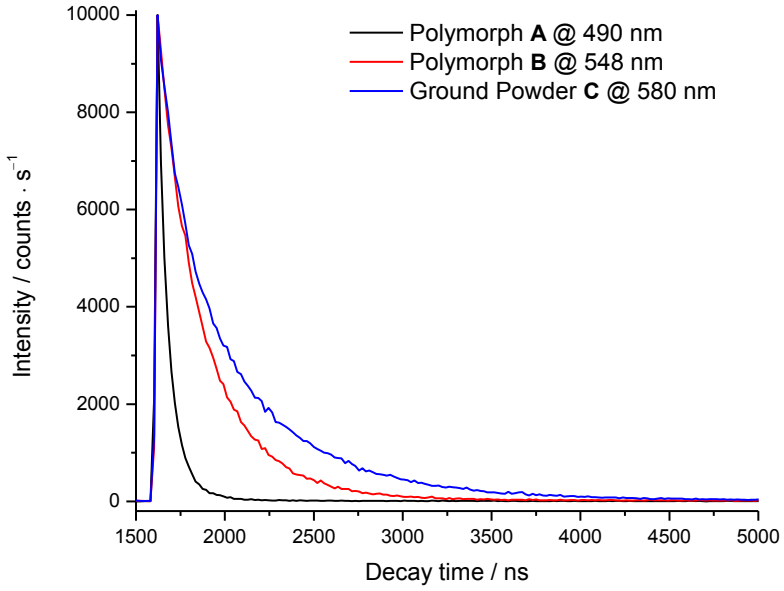

Figure S11. Luminescence decay curves of polymorph **A**, polymorph **B** and ground powder **C** measured at room temperature.

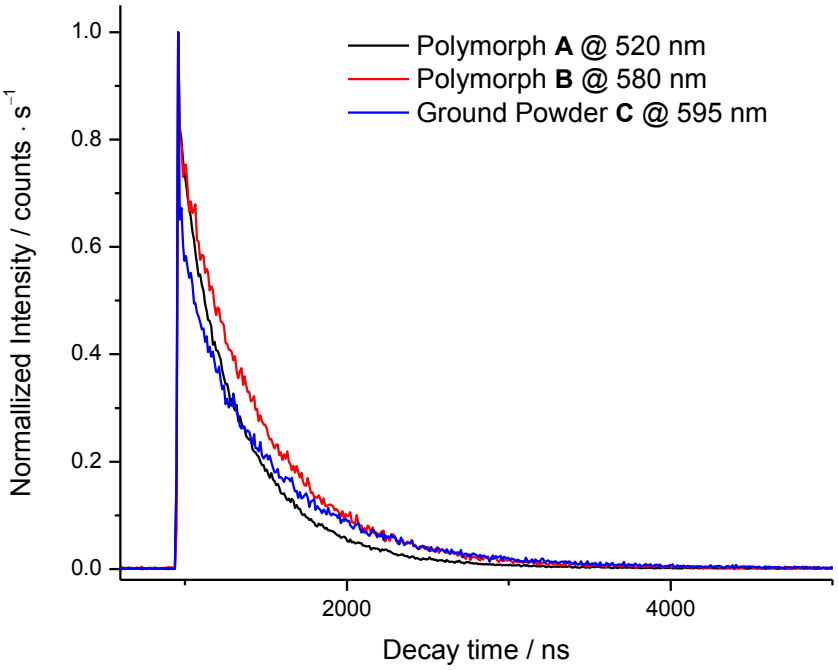

Figure S12. Luminescence decay curves of polymorph **A**, polymorph **B** and ground powder **C** measured at 77 K.

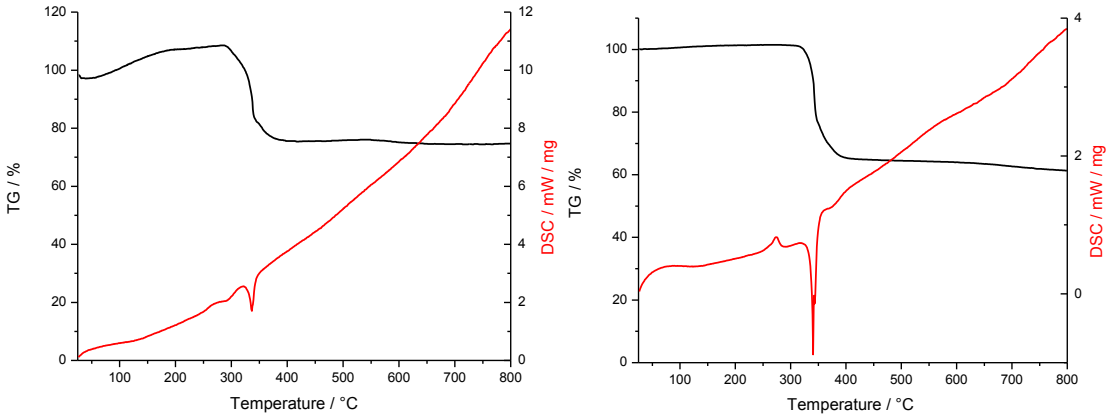

Figure S13. TGA-DSC measurement of polymorph **A** (left) and **B** (right) from room temperature to 800 ºC.

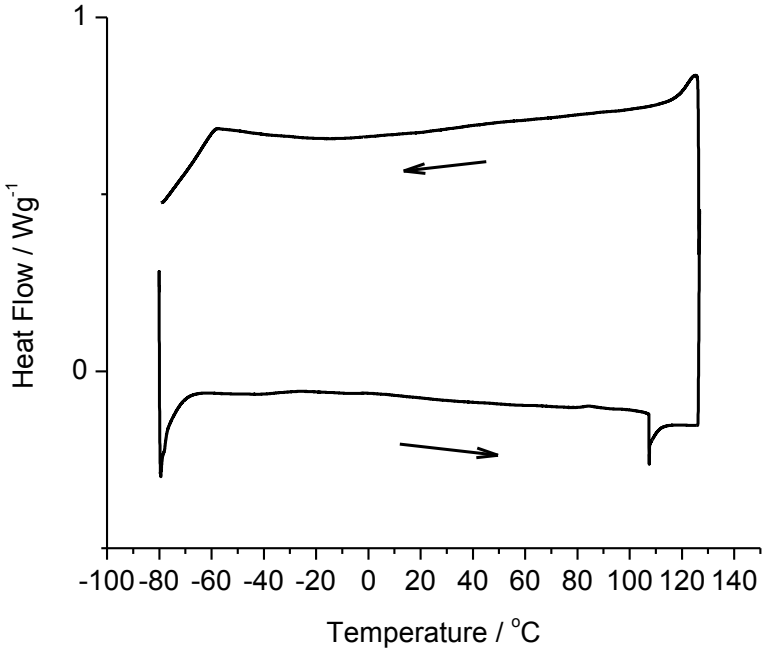

Figure S14. DSC measurement of polymorph **B** from -80 ºC to 127 ºC.

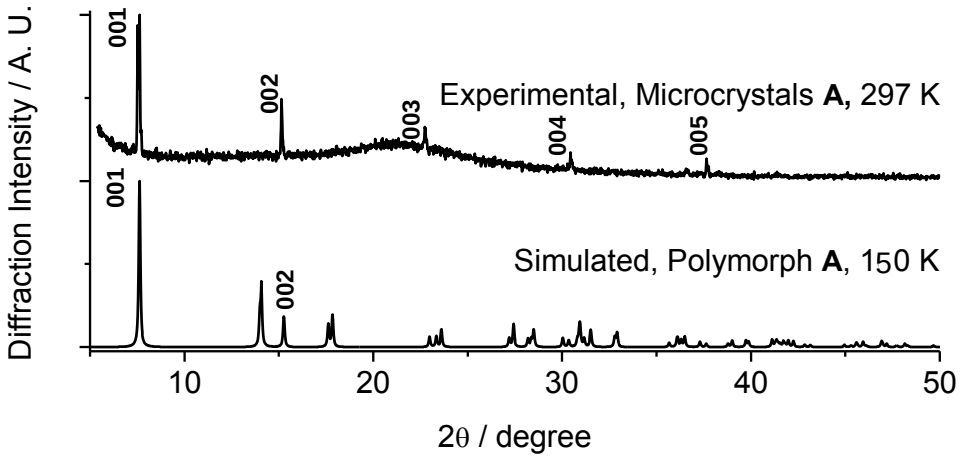

Figure S15. Comparisons between simulated PXRD pattern from single crystal structures of polymorphs **A** at 150 K and that recorded with bulky microcrystals of **A** at 297 K.

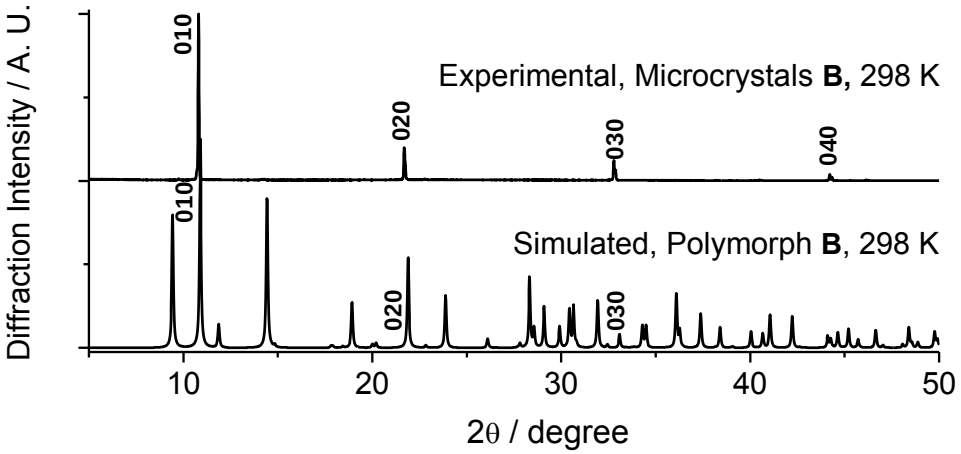

Figure S16. Comparisons between simulated PXRD pattern from single crystal structures of polymorphs **B** at 298 K and that recorded with bulky microcrystals of **B** at 297 K.

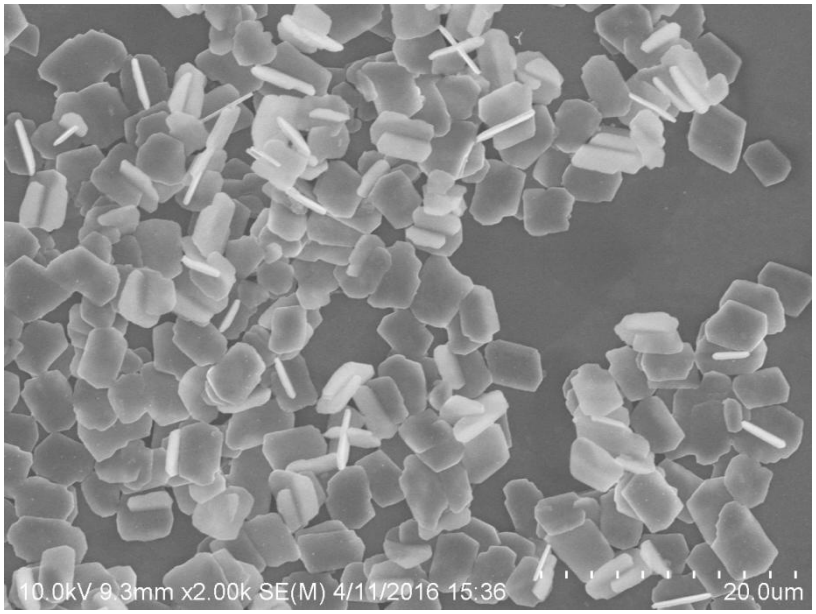

Figure S19. SEM image of double salt (polymorph **B**) made in water. Concentration of cation and anion was 5 mM.

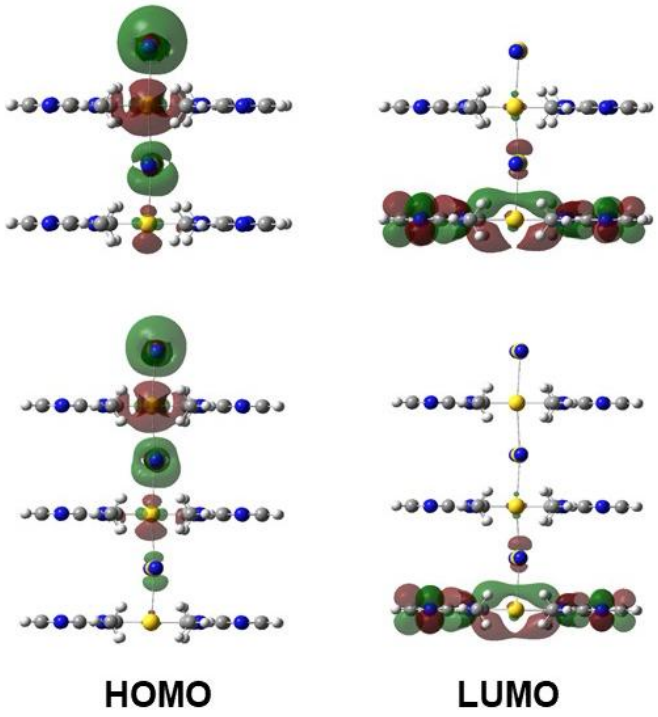

Figure S20. TD-DFT calculated frontier orbital diagram for tetranuclear and hexanuclear oligomers of $[Au(NHC)_2][Au(CN)_2]$.

Table S4. All calculated lowest-lying absorptions with the vertical excitation energies (nm), oscillator strength (*f*), and corresponding energy levels of HOMO and LUMO.

D/Å	A/ º	state	λ/nm	*f*	assign	HOMO/eV	LUMO/eV	energy gap/eV	total electron energy/a.u.
315	20	S1	380.7	0.065	H-L	-6.427	-2.655	3.772	-1437.67475
315	25	S1	382.0	0.065	H-L	-6.430	-2.671	3.759	-1437.67539
315	30	S1	383.2	0.064	H-L	-6.435	-2.688	3.747	-1437.67602
315	35	S1	384.2	0.063	H-L	-6.443	-2.705	3.738	-1437.67651
315	40	S1	385.0	0.063	H-L	-6.451	-2.722	3.729	-1437.67697
315	45	S1	385.8	0.062	H-L	-6.459	-2.738	3.721	-1437.67753
315	50	S1	386.6	0.061	H-L	-6.466	-2.753	3.713	-1437.67842
315	55	S1	387.5	0.061	H-L	-6.472	-2.767	3.705	-1437.67966
315	60	S1	388.7	0.061	H-L	-6.474	-2.781	3.693	-1437.68117
315	65	S1	390.1	0.061	H-L	-6.474	-2.793	3.681	-1437.68268
315	70	S1	391.6	0.061	H-L	-6.472	-2.804	3.668	-1437.68400
315	75	S1	392.8	0.061	H-L	-6.469	-2.813	3.656	-1437.68499
315	80	S1	393.7	0.061	H-L	-6.467	-2.818	3.649	-1437.68555
315	85	S1	394.0	0.061	H-L	-6.465	-2.820	3.645	-1437.68569
320	20	S1	365.0	0.070	H-L	-6.387	-2.468	3.919	-1437.36206
320	25	S1	366.3	0.070	H-L	-6.388	-2.484	3.904	-1437.36273
320	30	S1	367.8	0.070	H-L	-6.391	-2.503	3.888	-1437.36351
320	35	S1	369.4	0.070	H-L	-6.394	-2.524	3.870	-1437.36436
320	40	S1	371.1	0.069	H-L	-6.397	-2.545	3.852	-1437.36527
320	44	S1	371.8	0.069	H-L	-6.398	-2.554	3.844	-1437.36568
320	45	S1	372.9	0.068	H-L	-6.400	-2.566	3.834	-1437.36618
320	50	S1	374.7	0.067	H-L	-6.401	-2.586	3.815	-1437.36707
320	55	S1	376.8	0.066	H-L	-6.401	-2.606	3.795	-1437.36792
320	60	S1	378.8	0.065	H-L	-6.399	-2.624	3.775	-1437.36872
320	65	S1	380.8	0.064	H-L	-6.397	-2.641	3.756	-1437.36943
320	70	S1	382.6	0.064	H-L	-6.395	-2.655	3.740	-1437.37001
320	75	S1	383.9	0.064	H-L	-6.394	-2.667	3.727	-1437.37047
320	80	S1	384.8	0.064	H-L	-6.395	-2.675	3.720	-1437.37080
320	85	S1	385.1	0.064	H-L	-6.397	-2.680	3.717	-1437.37102
325	20	S1	376.7	0.037	H-L	-6.270	-2.481	3.789	-1437.43185
325	25	S1	378.7	0.037	H-L	-6.270	-2.500	3.770	-1437.43251
325	30	S1	381.2	0.036	H-L	-6.270	-2.524	3.746	-1437.43339
325	35	S1	393.9	0.035	H-L	-6.271	-2.550	3.721	-1437.43432
325	40	S1	386.6	0.035	H-L	-6.272	-2.575	3.697	-1437.43521
325	45	S1	389.4	0.034	H-L	-6.272	-2.600	3.672	-1437.43599
325	50	S1	392.1	0.034	H-L	-6.271	-2.623	3.648	-1437.43671
325	55	S1	394.7	0.033	H-L	-6.271	-2.644	3.627	-1437.43740
325	60	S1	397.1	0.033	H-L	-6.269	-2.663	3.606	-1437.43798
325	65	S1	399.3	0.033	H-L	-6.267	-2.680	3.587	-1437.43850
325	70	S1	401.2	0.033	H-L	-6.265	-2.693	3.572	-1437.43893
325	75	S1	402.7	0.033	H-L	-6.264	-2.704	3.560	-1437.43925
325	80	S1	403.8	0.033	H-L	-6.262	-2.711	3.551	-1437.43948
325	85	S1	404.4	0.033	H-L	-6.261	-2.715	3.546	-1437.43967

Computational details

All calculations were performed with Gaussian 09 suite of program[1] employing density functional theory (DFT) and time-dependent density functional theory (TDDFT). The hybrid functional B3LYP[2] with dispersion correction (D3)[3] with double zeta basis set (LanL2DZ[4] for Au and 6-31G(d)[5] for other atoms) was applied here. The initial structural units for computing were all derived from the X-ray crystal structures and partial freeze energy minimization was utilized in geometry optimization of ground state. The main structure of complex was frozen, and degree of freedom was only provided for the hydrogen atoms and the methyl groups. The singlet vertical excitation energy and corresponding electron transition as well as the frontier molecular orbital analysis was based on the ground state geometry. All selected excitations are the lowest-lying absorptions (S_0-S_1), which are the most credible results from calculation. In the crystal lattice, the structural changes of the molecules are limited, so we suggest that the singlet absorption has a corresponding relationship with the emission.

The anion-cation interaction energy was defined as below:

$$E_{int} = E_{complex\,salt} - (E_{anion} + E_{cation})$$

The basis set superposition error (BSSE) included in anion-cation interaction energy was achieved by using the counterpoise method. All calculations were done in vacuo.

1 M. J. Frisch, G. W. T., H. B. Schlegel, G. E. Scuseria, M. A. Robb, J. R. Cheeseman, G. Scalmani, V. Barone, B. Mennucci, G. A. Petersson, H. Nakatsuji, M. Caricato, X. Li, H. P. Hratchian, A. F. Izmaylov, J. Bloino, G. Zheng, J. L. Sonnenberg, M. Hada, M. Ehara, K. Toyota, R. Fukuda, J. Hasegawa, M. Ishida, T. Nakajima, Y. Honda, O. Kitao, H. Nakai, T. Vreven, J. A. Montgomery, Jr., J. E. Peralta, F. Ogliaro, M. Bearpark, J. J. Heyd, E. Brothers, K. N. Kudin, V. N. Staroverov, R. Kobayashi, J. Normand, K.

Raghavachari, A. Rendell, J. C. Burant, S. S. Iyengar, J. Tomasi, M. Cossi, N. Rega, J. M. Millam, M. Klene, J. E. Knox, J. B. Cross, V. Bakken, C. Adamo, J. Jaramillo, R. Gomperts, R. E. Stratmann, O. Yazyev, A. J. Austin, R. Cammi, C. Pomelli, J. W. Ochterski, R. L. Martin, K. Morokuma, V. G. Zakrzewski, G. A. Voth, P. Salvador, J. J. Dannenberg, S. Dapprich, A. D. Daniels, Ö. Farkas, J. B. Foresman, J. V. Ortiz, J. Cioslowski and D. J. Fox, Gaussian, Inc., Wallingford CT, *Gaussian, Inc.Wallingford CT*, **2009**.

2 A. D. Becke, *J. Chem. Phys.*, **1993**, *98*, 5648.

3 S. Grimme, J. Antony, S. Ehrlich and H. Krieg, *J. Chem. Phys.*, **2010**, *132*, 154104.

4 C. E. Check, T. O. Faust, J. M. Bailey, B. J. Wright, T. M. Gilbert and L. S. Sunderlin, *J. Phys. Chem. A*, **2001**, *105*, 8111.

5 P. C. Hariharan and J. A. Pople, *Theoretica Chimica Acta*, **1973**, *28*, 213.